(4) the collisional frequency factor, between pyrene molecules, decreasing significantly with increasing density.

Currently, we are investigating the pyrene system in supercritical CF_3H and C_2H_4. We shall report the results of these efforts in due time.

Acknowledgment. This work has been supported generously by the United States Department of Energy (DE-FGO2-90ER14143). Special thanks are also extended to Kevin S. Litwiler for helping with the development of the time-domain acquisition software. We also thank Gary Sagerman for his continued help with instrument construction and Robert A. Osteryoung for use of his computer for data analysis. Finally, we appreciate the viscosity tables sent to us by David L. Tomasko.

Registry No. CO_2, 124-38-9; pyrene, 129-00-0.

Negative Ion Photoelectron Spectroscopy of Coordinatively Unsaturated Group VI Metal Carbonyls: $Cr(CO)_3$, $Mo(CO)_3$, and $W(CO)_3$

Ashfaq A. Bengali, Sean M. Casey, Chun-Lin Cheng, Jonathan P. Dick, P. Thomas Fenn, Peter W. Villalta, and Doreen G. Leopold*,†

Contribution from the Department of Chemistry, University of Minnesota, Minneapolis, Minnesota 55455. *Received November 12, 1991*

Abstract: Photoelectron spectra are reported for $Cr(CO)_3^-$, $Mo(CO)_3^-$, and $W(CO)_3^-$ anions prepared from the corresponding metal hexacarbonyls in a flowing afterglow ion source. The 488-nm spectra were obtained at an electron kinetic energy resolution of 5 meV using a new apparatus with improved mass resolution, which is described in this report. The spectra exhibit transitions between the ground electronic states of the anions and the neutral molecules, and they show weak activity in the symmetric CO stretching, MC stretching, MCO bending, and CMC bending vibrational modes. The observed vibrational structure indicates that the anions, like the neutral molecules, have C_{3v} equilibrium geometries. Principal force constants estimated from the measured vibrational frequencies of the neutral molecules are consistent with stronger metal–ligand bonding in the coordinatively unsaturated tricarbonyls than in the corresponding hexacarbonyl complexes. Franck–Condon analyses of the spectra indicate only small differences between the equilibrium bond lengths and bond angles of the anions and the corresponding neutral molecules. Electron affinities of 1.349 ± 0.006 eV for $Cr(CO)_3$, 1.337 ± 0.006 eV for $Mo(CO)_3$, and 1.859 ± 0.006 eV for $W(CO)_3$ are obtained. The electron affinity pattern observed among the three group VI metal tricarbonyls is compared with characteristic trends within triads of transition metal atoms and within the coinage metal dimer series. This comparison, combined with the results of previously reported theoretical calculations, suggests that the extra electron in the $M(CO)_3^-$ anions occupies an sp hybrid orbital. Related studies of the atomic anions yield improved values for the electron affinities of Cr (0.675 ± 0.004 eV), Mo (0.747 ± 0.004 eV), and W (0.817 ± 0.004 eV).

I. Introduction

Coordinatively unsaturated metal carbonyls are of interest as active species in catalytic reactions,[1-4] as the building blocks of stable organometallic complexes,[5] and as computationally tractable benchmarks against which to test theoretical models of metal–carbonyl bonding.[6] Although unsaturated metal carbonyls have many features in common with their fully ligated counterparts, qualitative differences in their electronic structure and bonding are also expected. As the ligands are sequentially removed from a coordinatively saturated $M(CO)_n$ complex, the metal atom will return from its low-spin s^0d^m valence electron configuration in the complex to its ground-state configuration, which in general is high-spin s^2d^{m-2} or s^1d^{m-1}. These electronic structure changes can be accompanied by dramatic variations in chemical reactivity, metal–ligand bond strengths, and molecular structure. For example, among the neutral $Fe(CO)_n$ molecules, sequential metal–ligand bond strengths differ by an order of magnitude,[7,8] and reactivity toward CO varies by almost 3 orders of magnitude.[9,10] Theoretical studies[11,12] indicate that the bonding in some metal–carbonyl fragments deviates significantly from the traditional model, in which the metal–carbonyl bond is viewed as arising from ligand-to-metal σ donation and metal-to-ligand π back-donation.

We report here a study of gas-phase $Cr(CO)_3$, $Mo(CO)_3$, and $W(CO)_3$ and the corresponding anions by negative ion photoelectron spectroscopy. These systems provide an opportunity to compare the bonding for open d-shell metal carbonyls of the first, second, and third transition series at a degree of coordinative

† Presidential Young Investigator, 1988–1993.

(1) Cotton, F. A.; Wilkinson, G. *Advanced Inorganic Chemistry*; Wiley: New York, 1988. Collman, J. P.; Hegedus, L. S.; Norton, J. R.; Finke, R. G. *Principles and Applications of Organotransition Metal Chemistry*; University Science Books: Mill Valley, CA, 1987.

(2) Iwasawa, Y., Ed. *Tailored Metal Catalysts*; D. Reidel: Dordrecht, The Netherlands, 1986. Bailey, D. C.; Langer, S. H. *Chem. Rev.* **1981**, *81*, 109–148.

(3) Ugo, R., Ed. *Aspects of Homogeneous Catalysis*; D. Reidel: Dordrecht, The Netherlands, 1984; Vol. 5. Parshall, G. W. *Homogeneous Catalysis*; Wiley: New York, 1980.

(4) Geoffroy, G. L.; Wrighton, M. S. *Organometallic Photochemistry*; Academic Press: New York, 1979.

(5) Hoffmann, R. *Angew. Chem., Intl. Ed. Engl.* **1982**, *21*, 711–724.

(6) Veillard, A. *Chem. Rev.* **1991**, *91*, 743–766.

(7) Engelking, P. C.; Lineberger, W. C. *J. Am. Chem. Soc.* **1979**, *101*, 5569–5573.

(8) Sunderlin, L. S.; Wang, D.; Squires, R. R. *J. Am. Chem. Soc.* **1992**, *114*, 2788–2796.

(9) Ouderkirk, A.; Weitz, E. *J. Chem. Phys.* **1983**, *79*, 1089–1091. Seder, T. A.; Ouderkirk, A. J.; Weitz, E. *J. Chem. Phys.* **1986**, *85*, 1977–1986.

(10) Weitz, E. *J. Phys. Chem.* **1987**, *91*, 3945–3953.

(11) (a) Barnes, L. A.; Rosi, M.; Bauschlicher, C. W., Jr. *J. Chem. Phys.* **1990**, *93*, 609–624. (b) Blomberg, M.; Brandemark, U.; Johansson, J.; Siegbahn, P.; Wennerberg, J. *J. Chem. Phys.* **1988**, *88*, 4324–4333. (c) Bauschlicher, C. W., Jr.; Bagus, P. S.; Nelin, C. J.; Roos, B. O. *J. Chem. Phys.* **1986**, *85*, 354–364. (d) Bauschlicher, C. W., Jr. *J. Chem. Phys.* **1986**, *84*, 260–267. (e) Bauschlicher, C. W., Jr.; Bagus, P. S. *J. Chem. Phys.* **1984**, *81*, 5889–5898. (f) Bagus, P. S.; Nelin, C. J.; Bauschlicher, C. W., Jr. *J. Vac. Sci. Technol.* **1984**, *A2*, 905–909.

0002-7863/92/1514-5257$03.00/0

unsaturation intermediate between that of the bare metal atom and the saturated complex.

Previous spectroscopic studies of the group VI metal tricarbonyls have been limited to the measurement of CO stretching vibrational frequencies by infrared spectroscopy of the matrix-isolated[13] and gas-phase[10,14-16] molecules. Perutz and Turner[13] found that matrix-isolated $Cr(CO)_3$, $Mo(CO)_3$, and $W(CO)_3$ each exhibits two IR-active CO stretching modes, ruling out a planar D_{3h} structure. Intensity ratios observed for $Mo(CO)_3$ and its isotopic derivatives indicate a C_{3v} structure with a C–Mo–C bond angle of 105°.[13] The symmetric CO stretching vibrations of the three tricarbonyls in CH_4 matrices fall in the range 1975–1981 cm^{-1}, substantially reduced from the 2112–2117 cm^{-1} values observed[17] for the stable hexacarbonyls in solution. Gas-phase time-resolved infrared absorption studies of $Cr(CO)_3$ and $Mo(CO)_3$ by the Weitz,[10,14] Rosenfeld,[15] and Rayner[16] groups identified the more intense CO stretch of E symmetry at the frequency expected based on the matrix study, providing evidence that these molecules adopt a C_{3v} structure in the gas phase as well. These studies also found that bimolecular rate constants for CO addition to $Cr(CO)_n$ (n = 2–5) and $Mo(CO)_n$ (n = 3–5) were within an order of magnitude of the gas kinetic collision rate.[10,14-16] Since the $M(CO)_6$ complexes are known to have singlet ground states, and reactions requiring a change in spin multiplicity are expected to be relatively slow, these data suggest that $Cr(CO)_3$ and $Mo(CO)_3$ also have singlet ground states.

In other gas-phase experimental studies, the bond strengths of coordinatively unsaturated group VI metal carbonyls have been obtained by techniques involving excimer laser photolysis of the parent hexacarbonyls.[18-20] Two of these studies[18,20] found the $M(CO)_n$–CO (n = 3–5) bond dissociation energies each to be within 0.3 eV of the average energy required to dissociate the first three CO ligands from the corresponding metal hexacarbonyl complex. These results were interpreted as being consistent with the view that the metal center in $M(CO)_3$, like that in $M(CO)_6$, has a low-spin d^6 configuration.[18] Bond strengths of the $M(CO)_3^-$ anions have been estimated from appearance potential measurements.[21,22] Several ion cyclotron resonance studies of the photochemistry and chemical reactivity of $Cr(CO)_3^-$ have also been reported.[23-25] On the basis of a study of ion–molecule reactivity patterns, McElvany and Allison[24] predicted the electron affinity of $Cr(CO)_3$ to be less than that of a number of other metal carbonyls including $Fe(CO)_3$, whose electron affinity is known[7] to be 1.8 ± 0.2 eV.

Properties of group VI $M(CO)_3$ fragments adsorbed on metal oxide supports or encaged in zeolites have been investigated by several groups.[2,26-29] Metal oxide supported $Mo(CO)_3$ is believed to catalyze olefin metathesis[2,26,27] and allylic alkylation[27] reactions. Intrazeolite $Mo(CO)_3$ has been proposed as the active catalytic species in the stereoselective hydrogenation of butadiene and isomerization of 1,4-pentadiene.[28] The geometry and electronic structure of group VI metal tricarbonyls anchored in type-Y alkali metal zeolites have been investigated by infrared, EXAFS, and XPS techniques, and their spectroscopic properties have been contrasted with those of free $M(CO)_3$.[28,29]

Theoretical studies of the group VI tricarbonyls include several semiempirical calculations;[30-33] to our knowledge, no ab initio calculations have been reported to date. Although early calculations by Kettle[30] suggested planar D_{3h} geometries for all $M(CO)_3$ fragments in accord with the VSEPR rules, subsequent molecular orbital calculations by Burdett[31] and by Elian, Hoffmann, and co-workers[32] predicted low-spin d^6 $M(CO)_3$ molecules to adopt a pyramidal C_{3v} structure. Elian and Hoffmann predicted the ground state of $Cr(CO)_3$, for example, to have a C–Cr–C bond angle of 93° and a singlet d^6 configuration in which the six valence electrons occupy a set of three closely-spaced a_1 + e orbitals reminiscent of the low-lying t_{2g} set in the octahedral hexacarbonyl complex.[32] The driving force for this nonplanarity is the rapid stabilization of the a_1 (d_{z^2}) orbital (oriented along the C_{3v} symmetry axis) as the molecule bends, due to decreased metal–ligand σ repulsion and increased bonding with the carbonyl π^* orbitals.[31,32] Burdett also found the low-spin d^6 tricarbonyls to adopt a C_{3v} structure, but predicted planar or Jahn–Teller distorted geometries for states with high or intermediate spin.[31] These computational results, combined with the experimentally determined[13] C_{3v} geometry for matrix-isolated $Mo(CO)_3$, suggest that the neutral group VI tricarbonyls have singlet ground states, a conclusion also reached in the kinetics studies[10,14-16] described above. Thus, all theoretical and experimental results reported to date appear consistent with the notion that the addition of just three CO ligands to the metal atom (whose ground state is $^7S_3$, s^1d^5 for Cr and Mo and $^5D_0$, s^2d^4 for W) is sufficient to cause both promotion to an s^0d^6 configuration and complete pairing of the d electrons to give a singlet $M(CO)_3$ ground state.

Negative ion photoelectron spectroscopy[34,35] has several unique advantages as a method for studying neutral and anionic coordinatively unsaturated organometallic species. Since the selection rules for vibrational transitions are determined by Franck–Condon factors, it is often possible to observe vibrational states that are forbidden or weak in infrared spectroscopy. In particular, it is in principle possible to observe the bending and M–C stretching modes of the neutral molecule, which have thus far escaped detection for neutral binary (i.e., unsubstituted) metal tricarbonyls by other spectroscopic techniques. Negative ion photoelectron spectroscopy also allows the measurement of the electron affinity of the neutral molecule, a value that may be useful in understanding its reactivity toward electron-rich reagents. In addition, intensity ratios observed in the photoelectron spectra yield quantitative information concerning the change in molecular structure induced by addition of the extra electron.

Previous reports of organometallic species studied by negative ion photoelectron spectroscopy have been limited to $Fe(CO)_n$ (n

(12) Mavridis, A.; Harrison, J. F.; Allison, J. *J. Am. Chem. Soc.* **1989**, *111*, 2482–2487.
(13) Perutz, R. N.; Turner, J. J. *J. Am. Chem. Soc.* **1975**, *97*, 4800–4804.
(14) Seder, T. A.; Church, S. P.; Weitz, E. *J. Am. Chem. Soc.* **1986**, *108*, 4721–4728.
(15) Ganske, J. A.; Rosenfeld, R. N. *J. Phys. Chem.* **1989**, *93*, 1959–1963.
(16) Ishikawa, Y.; Brown, C. E.; Hackett, P. A.; Rayner, D. M. *J. Phys. Chem.* **1990**, *94*, 2404–2413.
(17) Jones, L. H.; McDowell, R. S.; Goldblatt, M. *Inorg. Chem.* **1969**, *8*, 2349–2363.
(18) Rayner, D. M.; Ishikawa, Y.; Brown, C. E.; Hackett, P. A. *J. Chem. Phys.* **1991**, *94*, 5471–5480.
(19) Venkataraman, B.; Hou, H.; Zhang, Z.; Chen, S.; Bandukwalla, G.; Vernon, M. *J. Chem. Phys.* **1990**, *92*, 5338–5362.
(20) Ganske, J. A.; Rosenfeld, R. N. *J. Phys. Chem.* **1990**, *94*, 4315–4318.
(21) Pignataro, S.; Foffani, A.; Grasso, F.; Cantone, B. *Z. Phys. Chem. (Munich)* **1965**, *47*, 106–113.
(22) Squires, R. R. *Chem. Rev.* **1987**, *87*, 623–646.
(23) Dunbar, R. C.; Hutchinson, B. B. *J. Am. Chem. Soc.* **1974**, *96*, 3816–3820.
(24) McElvany, S. W.; Allison, J. *Organometallics* **1986**, *5*, 416–426.
(25) Gregor, I. K. *Inorg. Chim. Acta* **1990**, *176*, 19–22; **1987**, *132*, 3–5; *Org. Mass Spectrom.* **1989**, *24*, 529–534; **1987**, *22*, 644–646; *J. Organomet. Chem.* **1987**, *329*, 201–208.
(26) Brenner, A.; Burwell, R. L., Jr. *J. Am. Chem. Soc.* **1975**, *97*, 2565–2566.
(27) Masuyama, Y.; Tomatsu, Y.; Ishida, K.; Kurusu, Y.; Segawa, K. *J. Catal.* **1988**, *114*, 347–353. Masuyama, Y.; Kurusu, Y.; Segawa, K. *J. Mol. Catal.* **1987**, *40*, 183–193.
(28) Okamoto, Y.; Kane, H.; Imanaka, T. *Chem. Lett.* **1988**, 2005–2008. Okamoto, Y.; Imanaka, T.; Asakura, K.; Iwasawa, Y. *J. Phys. Chem.* **1991**, *95*, 3700–3705.
(29) Ozkar, S.; Ozin, G. A.; Moller, K.; Bein, T. *J. Am. Chem. Soc.* **1990**, *112*, 9575–9586.
(30) Kettle, S. F. A. *Inorg. Chem.* **1965**, *4*, 1661–1663; *J. Chem. Soc. A* **1966**, 420–422.
(31) Burdett, J. K. *J. Chem. Soc., Faraday Trans. 2* **1974**, *70*, 1599–1613; *Inorg. Chem.* **1975**, *14*, 375–382.
(32) Elian, M.; Hoffmann, R. *Inorg. Chem.* **1975**, *14*, 1058–1076. Elian, M.; Chen, M. M. L.; Mingos, D. M. P.; Hoffmann, R. *Inorg. Chem.* **1976**, *15*, 1148–1155.
(33) Böhm, M. C.; Schmidt, P. C.; Sen, K. D. *J. Mol. Struct.* **1982**, *87*, 43–52.
(34) Lineberger, W. C. *Appl. At. Collision Phys.* **1982**, *5*, 239–254. Mead, R. D.; Stevens, A. E.; Lineberger, W. C. In *Gas Phase Ion Chemistry*; Bowers, M. T., Ed.; Academic Press: New York, 1984; Vol. III, pp 213–248.
(35) Ervin, K. M.; Lineberger, W. C. In *Advances in Gas Phase Ion Chemistry*; Adams, N. G., Babcock, L. M., Eds.; JAI Press: Greenwich, CT, Vol. I, in press.

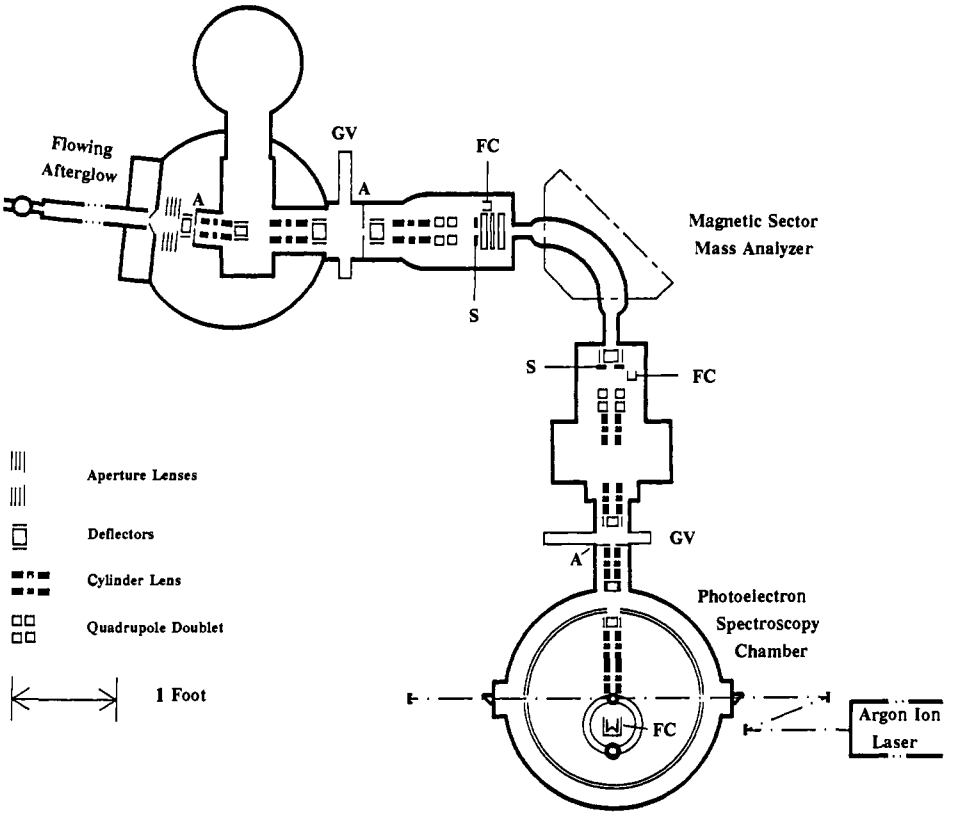

Figure 1. Block diagram of the negative ion photoelectron spectrometer: A = differential pumping aperture; GV = in-line gate valve; S = adjustable slit; FC = Faraday cup.

≤ 4)[7] and $Ni(CO)_n$ ($n \leq 3$).[36] Electron affinities measured in these studies were combined with negative ion bond strengths derived from previously reported[37] appearance potential data to yield the first complete sets of sequential metal–ligand bond strengths for neutral metal carbonyls. These studies also provided measurements of the symmetric CO stretching frequencies of the neutral molecules, as well as several frequencies for the negative ions. However, the 45–60 meV (360–480 cm^{-1}) instrumental resolution employed in these studies, and thermal broadening effects in the spectra of the 600–1000 K anions, prevented the measurement of low-frequency vibrational modes in the neutral molecules.

In the present study, we have exploited the dramatic improvements[35,38,39] that have been achieved in negative ion photoelectron spectroscopy during the decade following the earlier metal carbonyl work and have obtained spectra of room-temperature $Cr(CO)_3^-$, $Mo(CO)_3^-$, and $W(CO)_3^-$ anions at an instrumental resolution of 5 meV (40 cm^{-1}). We report the first measurements of M–C stretching, MCO bending, and CMC bending vibrational frequencies for any neutral binary metal tricarbonyl, as well as gas-phase values for the symmetric CO stretching vibrations previously observed[13] in matrix studies. Principal valence force constants are estimated on the basis of these results. Electron affinities are obtained and discussed in light of trends within triads of transition metal atoms and dimers. These measurements, combined with geometry changes upon electron detachment inferred from intensity ratios in the photoelectron spectra, yield new information concerning the electronic and molecular structures of the neutral group VI tricarbonyls and their negative ions.

II. Experimental Section

Spectra were obtained using a new negative ion photoelectron spectrometer diagrammed in Figure 1. Briefly, ions are prepared and thermalized in a flowing afterglow ion–molecule reactor. Negative ions sampled from the flowing afterglow are focused into a beam, accelerated, and mass analyzed by a 90° sector magnet. The mass-selected ion beam is then decelerated and crossed by the intracavity radiation of a continuous wave argon ion laser operated at 488 or 514 nm. A small solid angle of the resulting photoelectrons is energy analyzed by a hemispherical analyzer and detected by a position-sensitive detector. Since our apparatus differs in many of its construction details from previous instruments of this type,[34,35,38–42] a more complete description follows.

More specifically, the sample ions are produced in a flowing afterglow reactor[43] equipped with a 2.45-GHz microwave discharge ion source.[44] Although the ions may initially be formed in highly excited states, they are thermally equilibrated by 10^4–10^5 collisions with the helium buffer gas during their journey of several milliseconds down the field-free flow tube. The variable-length, 2 in. diameter stainless steel flow tube is normally operated at room temperature, but is equipped with an insulated jacket to allow cooling to liquid nitrogen temperature. At the end of the flow tube, most of the gas is pumped away by a 300 L/s Roots pump, while a small fraction of the ions and neutrals pass through a 2 mm diameter aperture in a molybdenum nosecone into a chamber maintained below 10^{-4} Torr by a 20 in. diameter diffusion pump. The large pumping capacity in this chamber permits the use of a mild supersonic expansion to further cool the ions. This option was not exploited in the present experiment, which employed a low (0.6 Torr) flow tube pressure.

On exiting the nosecone, the negative ions encounter a series of electrostatic lenses which focuses them into a beam and accelerates them

(36) Stevens, A. E.; Feigerle, C. S.; Lineberger, W. C. *J. Am. Chem. Soc.* **1982**, *104*, 5026–5031.
(37) Compton, R. N.; Stockdale, J. A. D. *Int. J. Mass Spectrom. Ion Phys.* **1976**, *22*, 47–55.
(38) Feigerle, C. S. Laser Photoelectron Spectroscopy Studies of Transition Metal Negative Ions. Ph.D. Thesis, University of Colorado, Boulder, CO, 1983.
(39) Leopold, D. G.; Murray, K. K.; Miller, A. E. S.; Lineberger, W. C. *J. Chem. Phys.* **1985**, *83*, 4849–4865.
(40) Breyer, F.; Frey, P.; Hotop, H. *Z. Phys. A: At. Nucl.* **1981**, *300*, 7–24.
(41) Ellis, H. B., Jr.; Ellison, G. B. *J. Chem. Phys.* **1983**, *78*, 6541–6558.
(42) Coe, J. V.; Snodgrass, J. T.; Freidhoff, C. B.; McHugh, K. M.; Bowen, K. H. *J. Chem. Phys.* **1986**, *84*, 618–625.
(43) Ferguson, E. E.; Fehsenfeld, F. C.; Schmeltekopf, A. L. *Adv. At. Mol. Phys.* **1969**, *5*, 1–56. Bierbaum, V. M.; Ellison, G. B.; Leone, S. R. In *Gas Phase Ion Chemistry*; Bowers, M. T., Ed.; Academic Press: New York, 1984; Vol. III, pp 1–39. Smith, D.; Adams, N. G. In *Gas Phase Ion Chemistry*; Bowers, M. T., Ed.; Academic Press: New York, 1979; Vol. I, pp 1–44. Graul, S. T.; Squires, R. R. *Mass Spectrom. Rev.* **1988**, *7*, 263–358.
(44) Fehsenfeld, F. C.; Evenson, K. M.; Broida, H. P. *Rev. Sci. Instrum.* **1965**, *36*, 294–298. Cavity #5 was scaled up for a 1 in. diameter tube.

from the ground potential of the flow tube to 1200 V for mass analysis. This lens stack includes several closely-spaced 2 in. inner diameter (i.d.) aperture lenses in the first diffusion-pumped chamber, followed by three $1-1^1/_4$ in. i.d. three-element thick-walled cylinder lenses in subsequent chambers. A 6° bend in the ion beam line prevents on-axis neutrals from entering the mass analysis chamber. As the ions pass from the nosecone to the mass analyzer, three stages of differential pumping (provided by the 20-in. diffusion pump and two 6-in. diffusion pumps) reduce the ambient pressure to 1×10^{-7} Torr. A 5 in. diameter bellows connects the vacuum chambers on either side of the magnet tube, allowing them both to be pumped by the same 6-in. diffusion pump.

The mass analyzer in this instrument is an 8 in. radius 90° sector electromagnet, which takes the place of the Wien velocity filters used for mass selection in previous[34,35,38-42] continuous beam negative ion photoelectron spectrometers. In our instrument, ions entering the entrance slit of the mass analyzer are first focused by an electrostatic DC quadrupole doublet lens[45] to improve ion transmission through the narrow (8 mm high) magnet tube. The electromagnet can be scanned to record a mass spectrum or fixed at the field required to pass only ions of a specific mass into the photoelectron spectroscopy chamber. The entrance and exit slits of the mass analyzer are externally selectable from 2 mm, giving near-unity ion transmission efficiency through the magnet tube and moderate mass resolution, to 0.2 mm, giving better mass resolution with up to a 10-fold loss in ion transmission efficiency, depending on focusing conditions. With the narrowest slits, the measured mass resolving power of this system is $m/\Delta m = 400$ (where Δm is the full width at half maximum of a peak at mass m). This result represents a 10-fold improvement over the mass resolution typically obtained in instruments of this type using Wien filters.

The ion beam emerging from the exit slit of the mass analyzer is reconverted to cylindrical symmetry by a second quadrupole doublet lens and then passed through two 1 in. i.d. three-element cylinder lenses. These optics partially decelerate the ions and focus them into the photoelectron spectroscopy chamber. In this ion-pumped high vacuum chamber, the ions pass through three additional sets of $^5/_8$ in. i.d. three-element cylinder lenses, which decelerate them to 20 V to increase their interaction time with the laser and to reduce kinematic broadening in the photoelectron spectra. This series of deceleration lenses also refocuses the ion beam to a 1–2 mm diameter spot at the intersection point with the laser beam. The requirement of refocusing the entire mass-selected ion beam passing through the exit slit of the mass analyzer to a tight spot at the laser crossing was the main reason that we chose to use a magnetic sector, which preserves a high ion beam optical quality, rather than a quadrupole mass filter. Voltages applied to all of the electrostatic ion optics in the instrument, and to the eight sets of vertical and horizontal deflectors distributed along the ion beam line to provide slight steering corrections, are controlled by external potentiometers. The potentiometers are manually adjusted to focus the ion beam at the laser crossing point (as indicated by the image on an $x-y$ oscilloscope which monitors the two-dimensional electron detector output) and to optimize the ion beam current detected by a sensitive Faraday cup in the photoelectron spectroscopy chamber.

The argon ion laser (Coherent Innova 200-20/4) is operated as a four mirror folded cavity resonator, so that the spectroscopy chamber, which is equipped with Brewster angle MgF_2 windows, can reside inside the laser cavity. This intracavity technique provides high circulating powers of ~100 W on a single line with a tight, 0.2 mm diameter focus at the ion beam–laser beam crossing point. A high laser power density is essential in this experiment, in view of the small cross sections characteristic of photodetachment processes ($\sim 10^{-18}$ cm^2) and the low sample ion currents typically obtained with the flowing afterglow ion source (1–100 pA). In the experiments reported here, the argon ion laser was tilted at the "magic angle"[46] to provide a polarization yielding signal intensities proportional to average photodetachment cross sections, independent of the angular momentum of the orbital from which the photoelectron is detached.

Our electron kinetic energy analyzer is modeled after the recent high-resolution design by Feigerle and Lineberger.[35,38] A small fraction of the photoelectrons is sampled at right angles to the plane of the ion and laser beams through a molybdenum aperture with a 3° half-angle of acceptance. The sampled electrons then pass through two $^1/_2$ in. i.d. three-element molybdenum cylinder lenses that accelerate or decelerate them to the transmission energy of an electrostatic hemispherical energy analyzer and focus the electron beam at the analyzer entrance plane. Application of DC voltages to the two hemispheres spatially disperses the electrons according to their kinetic energies. The OFHC copper hemispheres have a 3-in. average radius and a $^3/_4$-in. gap and are normally operated at a transmission energy of 1.5 V. The central $^5/_{16}$ in. of the dispersed electron beam exiting the hemispheres, typically corresponding to an energy window of 80 meV, then passes through two sets of 1 in. i.d. three-element cylinder lenses. This lens stack accelerates the electrons to 300 V and images them onto a 1 in. radius position-sensitive detector (Quantar Technology 3391A) consisting of five microchannel plates followed by a resistive anode. The entire electron spectrometer is enclosed in two large (~20-in. diameter) nested, capped Co-Netic magnetic shielding cylinders, which reduce external magnetic fields to about 1 mG near the analyzer. Only totally nonmagnetic metals, such as molybdenum, copper, aluminum, and titanium, were used in the construction of analyzer components.

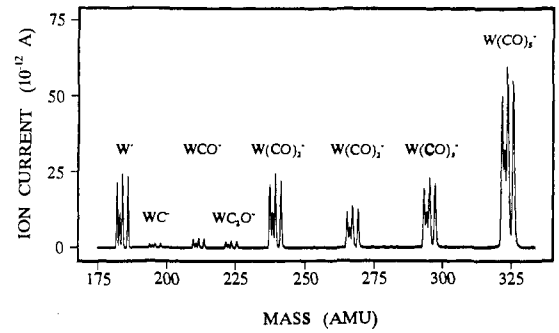

Figure 2. Mass spectrum of $W(CO)_n^-$ (n = 0–5) anions prepared in a flowing afterglow ion source. Each ion displays a quartet of peaks due to the four most abundant isotopes of W between 182 and 186 amu. The mass resolving power ($m/\Delta m$, FWHM) here is about 400.

The output of the electron detector is digitized (Quantar Technology Position Computer 2401) and then transmitted to a laboratory computer (IBM-AT type) for signal averaging. This computer also controls the voltages applied to the hemispheres and to the cylinder lenses nearest them via three 16-bit digital-to-analog converters (Analog Devices AD1147). Voltages applied to five additional electron lens elements are also computer controlled via Kepco Series SN500 12-bit voltage programmers interfaced to PCX-MAT power supplies. Spectra are typically obtained by collecting data for an 80-meV window for 5 s, then stepping the electron lens and hemispherical analyzer voltages so as to shift the energy window by 15–35 meV, and repeating the process until the entire electron kinetic energy range of interest (up to 2.54 eV at 488 nm) has been covered. The individual scans over the entire energy range, each of several minutes duration, are then averaged together to yield the final photoelectron spectrum, which typically represents 2–8 h of signal averaging time. This procedure averages out variations in laser power and ion current that may occur during the scan and allows the measurement of accurate relative transition intensities in the electron kinetic energy region above 0.3 eV, the region of interest in the present study. Peak intensities at lower energies are suppressed by the reduced sensitivity of the analyzer to very low-energy electrons.

The best resolution (FWHM) that we have obtained on this apparatus thus far is 3.0 meV, as measured by Lorentzian fits to peaks observed in the spectrum of W^-. The spectra reported here were obtained at 5-meV (40 cm^{-1}) resolution. Absolute electron kinetic energies are calibrated with respect to O^-, whose electron detachment energy is accurately known.[47] When performing these calibrations, low O^- and sample ion beam currents (<10 pA) are used to minimize charging effects or contact potential shifts in the analyzer. Use of significantly higher ion currents (>100 pA) has been found to produce energy shifts of several millielectronvolts. The relative electron kinetic energy scale is calibrated against fine structure splittings[48] observed in the W^- photoelectron spectrum, typically revealing a small linear energy scale compression factor of 0.2% or less. Both calibrations are performed immediately preceding and/or following the collection of a new photoelectron spectrum, without intermediate tuning of the ion optics. In addition to these two corrections, obtaining accurate electron kinetic energies requires converting the measured laboratory energies to the center-of-mass frame. With these procedures, splittings measured in the photoelectron

(45) Giese, C. F. *Rev. Sci. Instrum.* **1959**, *30*, 260–261. Lu, C.-S.; Carr, H. E. *Rev. Sci. Instrum.* **1962**, *33*, 823–824.
(46) Cooper, J.; Zare, R. N. *J. Chem. Phys.* **1968**, *48*, 942–943.
(47) Hotop, H.; Lineberger, W. C. *J. Phys. Chem. Ref. Data* **1985**, *14*, 731–750. Electron affinities given in section V, part A include more recent measurements for Fe and Co (Leopold, D. G.; Lineberger, W. C. *J. Chem. Phys.* **1986**, *85*, 51–55), Cu (ref 60), Pd (Ho, H.; Ervin, K. M.; Polak, M. L.; Gilles, M. K.; Lineberger, W. C. *J. Chem. Phys.* **1991**, *95*, 4845–4853), Cr, Mo, and W (this work).
(48) Moore, C. E. *Atomic Energy Levels*; National Bureau of Standards No. 467; NBS: Washington, DC, 1958; Vols. I–III.

spectra of Cr^-, Mo^-, and other atomic anions are found to agree with the known values[48] to ±5 cm^{-1} for electron kinetic energies above 0.3 eV, the region of interest in the present study. Absolute electron kinetic energies measured for well-resolved peaks in different experiments employing different ion optics settings and analyzer transmission energies are in general found to be reproducible to ±2 meV.

III. Results

Figure 2 shows a typical mass spectrum of $W(CO)_n^-$ anions prepared in the flowing afterglow source. The stable $W(CO)_6$ precursor was added at its room-temperature vapor pressure just downstream of the microwave discharge cavity. The microwave cavity was mounted on the axis of a 12 in. long flow tube and was operated at 30 W. The helium flow was regulated at 9 standard liters per minute, producing a flow tube pressure of 0.6 Torr. Ion currents for the most abundant (31%) ^{184}W isotopes, as detected by the Faraday cup in the photoelectron spectroscopy chamber, were approximately 60 pA for $W(CO)_5^-$, 25 pA for $W(CO)_4^-$, $W(CO)_2^-$, and W^-, 15 pA for $W(CO)_3^-$, and 3 pA for WCO^-. Small amounts of WC^- and WC_2O^- were also detected.

Mass spectra obtained for $Cr(CO)_6$ or $Mo(CO)_6$ precursors under the same flow tube conditions also produced a distribution of $M(CO)_n^-$ anions, although their relative abundances differed. For example, use of a $Cr(CO)_6$ precursor yielded, for the most abundant (84%) ^{52}Cr isotope, 1 nA of $Cr(CO)_5^-$, 250 pA of $Cr(CO)_4^-$, 20 pA of $Cr(CO)_3^-$, 1 pA of $Cr(CO)_2^-$, 0.05 pA of $CrCO^-$, and 3 pA of Cr^-. Small quantities of Cr_2^- anions[49] and $Cr_2(CO)_n^-$ species were also observed. For $Mo(CO)_6$, the same flow tube conditions yielded, for the most abundant (24%) ^{98}Mo isotope, 120 pA of $Mo(CO)_5^-$, 40 pA of $Mo(CO)_4^-$, 1 pA of $Mo(CO)_3^-$, 14 pA of $Mo(CO)_2^-$, <0.1 pA of $MoCO^-$, and 4 pA of Mo^-.

Photoelectron spectra obtained in these studies for the atomic metal anions yielded electron affinities of 0.675 ± 0.004 eV for Cr, 0.747 ± 0.004 eV for Mo, and 0.817 ± 0.004 eV for W. These values represent slightly more precise versions of previous literature measurements[50] obtained at 55-meV resolution. The quoted experimental uncertainties include the aforementioned ±0.002 eV reproducibility in absolute electron energies measured on our apparatus.

Figures 3–5 show photoelectron spectra obtained at 488 nm for the $Cr(CO)_3^-$, $Mo(CO)_3^-$, and $W(CO)_3^-$ anions. The spectra of the three group VI tricarbonyls are quite similar in general appearance, but are shifted in absolute energy. Each spectrum exhibits several peaks arising from photodetachment transitions from the ground electronic state of the anion to different vibrational levels of the ground electronic state of the neutral $M(CO)_3$ molecule. Scans over the entire electron kinetic energy range of 0–2.540 eV revealed no additional features due to photodetachment from $M(CO)_3^-$ anions, although very weak features attributed to anionic photofragments were observed, as discussed below.

The most intense peak in each spectrum, which appears at high electron kinetic energy (eKE), can readily be assigned as the origin band, corresponding to the "0–0 transition" between the zero-point vibrational levels of the anion and the neutral molecule. Lorentzian fits to the spectra indicate origin band positions of 1.191 eV eKE for $Cr(CO)_3^-$, 1.203 eV for $Mo(CO)_3^-$, and 0.681 eV for $W(CO)_3^-$. The widths of these peaks are 7–8 meV (FWHM), which is significantly greater than the 5 meV width observed for atomic transitions under the same instrumental conditions. This degree of broadening in the molecular spectra is not likely to be due to rotational effects: our calculations based on estimates for the neutral and anion geometries discussed in section IV indicate that unresolved rotational structure will not broaden the observed origin band (or shift its position) by more than 1 meV for these room-temperature anions.

Rather, the observed broadening of the origin peak, and of the other peaks in the spectrum, is most likely due to unresolved vibrational sequence bands. A rough calculation assuming that the $M(CO)_3$ systems have three low-frequency (~100 cm^{-1}) CMC bending modes, nine modes involving MCO bending and MC stretching with approximately the frequencies reported below, and three CO stretching modes suggests that fewer than 3% of the $M(CO)_3^-$ anions will be in the zero-point vibrational level at room temperature. Small differences between the anion and neutral molecule vibrational level spacings, causing $\Delta v = 0$ transitions from vibrationally excited anions to be somewhat shifted from that of the true 0–0 transition, could then easily result in the observed broadening of the origin band. This unresolved sequence

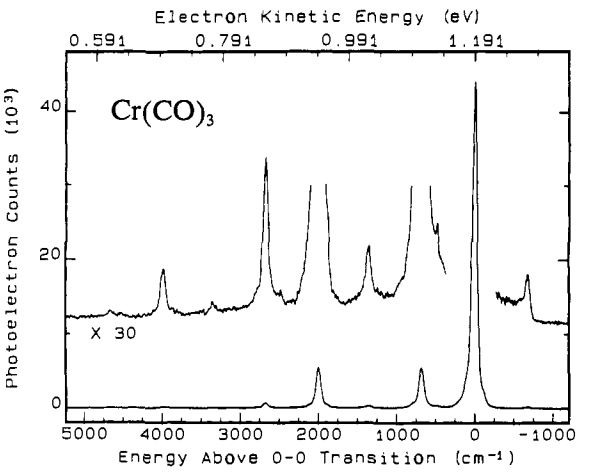

Figure 3. $Cr(CO)_3^- \rightarrow Cr(CO)_3 + e^-$ photoelectron spectrum at 488 nm (2.540 eV).

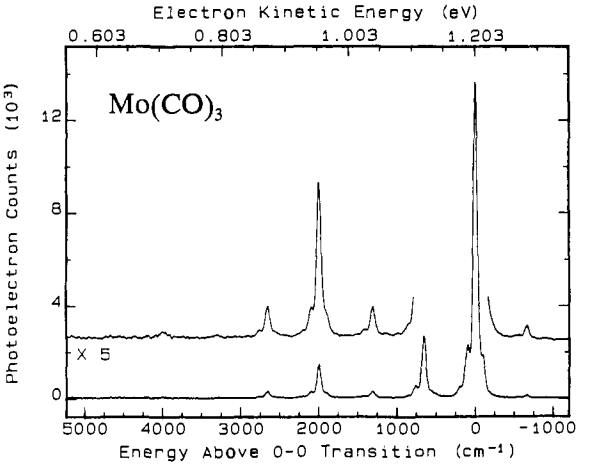

Figure 4. $Mo(CO)_3^- \rightarrow Mo(CO)_3 + e^-$ photoelectron spectrum at 488 nm (2.540 eV).

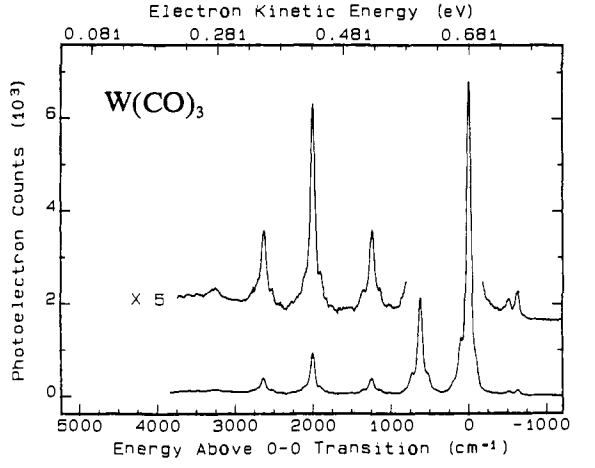

Figure 5. $W(CO)_3^- \rightarrow W(CO)_3 + e^-$ photoelectron spectrum at 488 nm (2.540 eV).

(49) Casey, S. M.; Villalta, P. W.; Bengali, A. A.; Cheng, C.-L.; Dick, J. P.; Fenn, P. T.; Leopold, D. G. *J. Am. Chem. Soc.* **1991**, *113*, 6688–6689.
(50) Feigerle, C. S.; Corderman, R. R.; Bobashev, S. V.; Lineberger, W. C. *J. Chem. Phys.* **1981**, *74*, 1580–1598.

structure could also produce a small shift between the true 0–0 transition and the observed origin band position.

Adiabatic electron affinities for the neutral $M(CO)_3$ molecules can be simply obtained by subtracting the observed origin band positions from the 2.540-eV photon energy. The resulting electron affinities are 1.349 ± 0.006 eV for $Cr(CO)_3$, 1.337 ± 0.006 eV for $Mo(CO)_3$, and 1.859 ± 0.006 eV for $W(CO)_3$. The quoted uncertainties include an estimated contribution from the unresolved sequence structure discussed above. The former value is surprisingly close to the 1.19-eV electron affinity predicted for $Cr(CO)_3$ by an INDO calculation.[33]

Each spectrum also exhibits transitions from the ground vibrational level of the anion to excited vibrational levels of the neutral molecule, which produce peaks to the left (low eKE) side of the origin band. The spacings between these peaks and the origin band provide measurements of vibrational frequencies in the neutral molecule. The relative intensities of these vibrational transitions are determined by the Franck–Condon overlap of the vibrational wave functions of the anion and the neutral molecule. As a result, a vibrational mode which corresponds to a change in equilibrium geometry between the anion and neutral will appear active in the spectrum, and the extent of this activity provides a quantitative signature of the magnitude of the geometry change.

It is evident from a casual inspection of Figures 3–5 that the $M(CO)_3^-$ photoelectron spectra show only weak vibrational activity, an indication that the equilibrium structures of the anions are very similar to those of the corresponding neutral molecules. The neutral C_{3v} molecules have four totally symmetric (A_1) vibrational modes, and their expected frequencies correspond to those of the four vibrational modes observed to be active in the $M(CO)_3$ spectra, as is described below. Therefore, it appears reasonable to assign the active modes as A_1 vibrations. This assignment implies that the group VI $M(CO)_3^-$ negative ions also have C_{3v} equilibrium geometries.

As shown in Figures 3–5, each $M(CO)_3^-$ spectrum displays a prominent peak 2000 ± 10 cm^{-1} above the 0–0 transition. This interval can readily be assigned as the symmetric CO stretching frequency in the neutral molecule. The $Cr(CO)_3^-$ and $Mo(CO)_3^-$ spectra also exhibit weaker peaks at 3990 cm^{-1} due to transitions to $v = 2$ of this mode. The corresponding overtone would appear near 0.185 eV eKE in the $W(CO)_3^-$ spectrum, but it is not detected due, in part, to the reduced sensitivity of our instrument at low electron energies.

The symmetric CO stretch was previously observed in CH_4 matrices by Perutz and Turner[13] at 1979 cm^{-1} for $Cr(CO)_3$, 1981 cm^{-1} for $Mo(CO)_3$, and 1975 cm^{-1} for $W(CO)_3$. For $Cr(CO)_3$ and $Mo(CO)_3$, the frequency of the CO stretch of E symmetry is increased by 21–29 cm^{-1} on going from the CH_4 matrix to the gas phase.[10,14-16] Thus, the 2000 ± 10 cm^{-1} frequencies observed here for the A_1 modes fall in the range expected on the basis of the previously reported matrix values and matrix-to-gas phase shifts. This excellent agreement provides further support for the conclusion that the neutral molecules adopt a C_{3v} structure in the gas phase as well as in matrices.

The second active vibrational mode in the photoelectron spectra gives rise to prominent peaks 680 ± 10, 660 ± 10, and 620 ± 10 cm^{-1} above the 0–0 transition for $Cr(CO)_3$, $Mo(CO)_3$, and $W(CO)_3$, respectively. These intervals, which again correspond to fundamental vibrational frequencies in the neutral molecules, are in the region expected for MCO bending and MC stretching vibrations.[51] The $v = 2$ overtone, and combination bands involving 1 or 2 quanta of excitation in this mode and 1 or 2 quanta of the CO stretch, is also observed in each spectrum. These overtone and combination bands exhibit no detectable anharmonicity at our resolution and have approximately the intensities expected on the basis of harmonic Franck–Condon fits to the relative intensities of the fundamental and origin bands. The fundamental, overtone, and combination bands involving these two modes account for all of the well-resolved peaks observed above the 0–0 transitions in the three spectra.

In the $Cr(CO)_3^-$ spectrum, a third vibrational mode is observed as a weak shoulder to the right of the 680 cm^{-1} peak, 480 ± 20 cm^{-1} above the 0–0 transition. This region of the spectrum is shown more clearly in Figure 6. This shoulder is not due to a transition from a 200 cm^{-1} excited anion state to the 680 cm^{-1} neutral molecule vibrational state, since corresponding hot bands are not observed for the origin and other prominent peaks in the spectrum. Rather, we assign this shoulder to a third vibrational mode with a fundamental frequency of 480 ± 20 cm^{-1} in neutral $Cr(CO)_3$. This frequency, as well, falls in the range expected for MCO bending and MC stretching vibrations.[51] This mode also appears in combination with the CO stretch, producing the weak

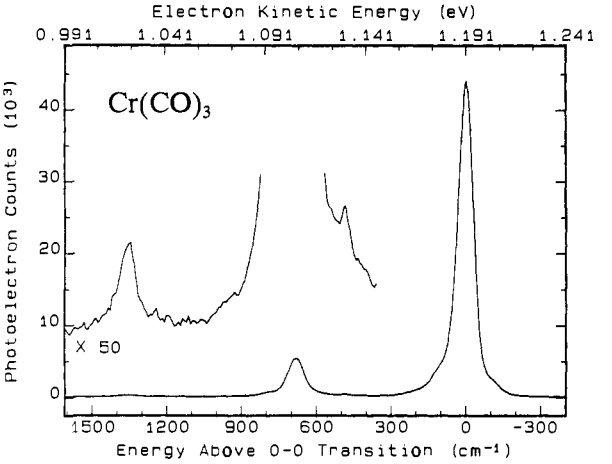

Figure 6. Expanded view of the 488-nm $Cr(CO)_3^- \rightarrow Cr(CO)_3 + e^-$ spectrum.

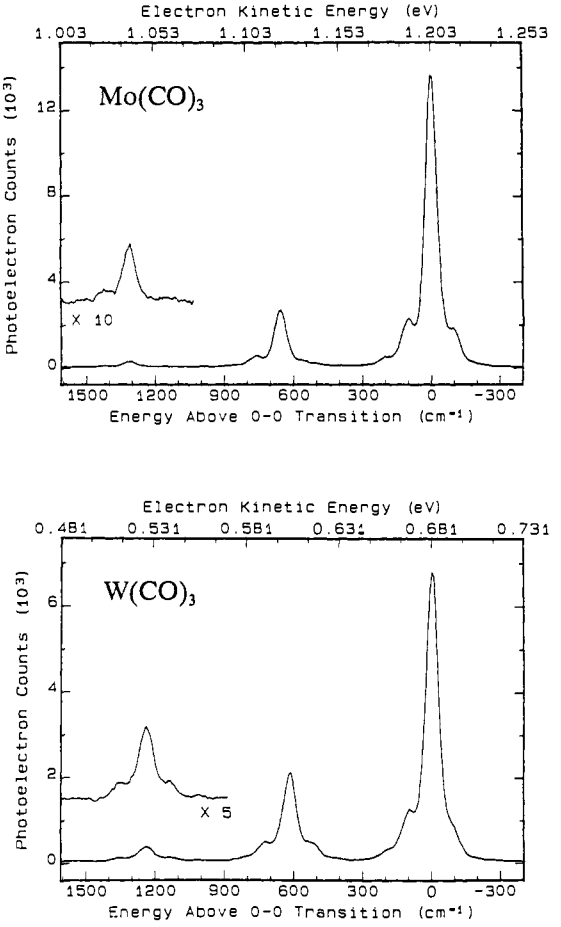

Figure 7. Expanded views of the $Mo(CO)_3^- \rightarrow Mo(CO)_3 + e^-$ and $W(CO)_3^- \rightarrow W(CO)_3 + e^-$ photoelectron spectra obtained at 488 nm.

(51) Braterman, P. S. *Metal Carbonyl Spectra*; Academic Press: London, 1975.

peak seen 2480 ± 20 cm^{-1} above the 0–0 transition in Figure 3.

The fourth and last active vibrational mode observed in this series of molecules appears as a weak shoulder 100 ± 20 cm^{-1} from the origin bands. As shown in Figure 7, these shoulders are most pronounced in the $Mo(CO)_3^-$ and $W(CO)_3^-$ spectra, which also display weak $v = 2$ overtones. This low-frequency mode is in the region expected for CMC bending vibrations. Shoulders observed 100 ± 20 cm^{-1} to the right of the origin bands are due to transitions from excited CMC bending levels in the anions. Combination bands involving the CMC bend in the neutral molecule, and sequence bands due to transitions from the excited 100 ± 20 cm^{-1} anion level, are also observed as shoulders on the other strong peaks in each spectrum.

The possibility that the shoulder observed in the $W(CO)_3^-$ spectrum 520 cm^{-1} above the origin band might reflect the activity of the same vibrational mode that gives rise to the 480 cm^{-1} peak in the $Cr(CO)_3^-$ spectrum was rejected for the following reason. A shoulder is also observed at 1900 cm^{-1}, and its intensity relative to that of the 2000 cm^{-1} peak is about the same as that of the 520 cm^{-1} shoulder relative to the 620 cm^{-1} peak. The former shoulder must be due to a transition from the excited 100 cm^{-1} anion level to the 2000 cm^{-1} level in the neutral molecule. The alternative assignment, to a combination band involving two quanta of the 620 cm^{-1} mode and one quantum of a 520 cm^{-1} mode, would produce a peak at ~1760 cm^{-1}, 140 cm^{-1} from the observed shoulder. Although the shoulders on the 620 and 2000 cm^{-1} peaks are both about twice as intense as would be expected on the basis of harmonic Franck–Condon fits to the relative intensities of the origin band and its associated 100 cm^{-1} hot band, this enhancement is apparently not due to the activity of a 520 cm^{-1} mode.

Additional features due to transitions from vibrationally excited anions are observed to the right of the origin bands in the 30× and 5× expansions shown in Figures 3–5. The positions of these hot bands give ion vibrational frequencies of 680 ± 10 cm^{-1} for $Cr(CO)_3^-$, 660 ± 10 cm^{-1} for $Mo(CO)_3^-$, and 630 ± 10 cm^{-1} for $W(CO)_3^-$. These values are equal to those in the corresponding neutral molecules within the quoted experimental uncertainties. Franck–Condon analyses of the spectra indicate that these hot bands have approximately the intensities expected for room-temperature anions.

In the $W(CO)_3^-$ spectrum, an additional peak is observed at 0.745 eV eKE, 520 cm^{-1} to the right of the origin band. Although this feature also has the appearance of a vibrational hot band, its behavior when the anion temperature is reduced does not support this assignment. When the flow tube is cooled with liquid nitrogen, the intensity of the 630 cm^{-1} hot band, relative to that of the origin, decreases by at least a factor of 5, yet the relative intensity of the peak in question does not change appreciably. A possible alternative assignment for the 0.745-eV peak is to a two-photon process involving photodissociation of $W(CO)_3^-$, followed by electron detachment from an anionic photofragment such as $W(CO)_2^-$ or WCO^-. The relative intensity of this feature does not show the quadratic dependence on laser power that would provide an unambiguous signature of such a process. However, this observation does not eliminate the possibility of a two-photon process, since it is possible that the photodissociation step is nearly saturated. Some support for such a mechanism is obtained from our preliminary scans of the WCO^- photoelectron spectrum, in which the two most intense peaks occur at 0.735 ± 0.006 and 0.754 ± 0.006 eV eKE, both very close to the 0.745-eV peak observed here. Excess energy in a WCO^- photofragment, which would not be collisionally relaxed in the ultrahigh vacuum photoelectron spectroscopy chamber, might account for a small shift in peak position from that of the room-temperature anion.

Additional evidence for photofragmentation is found in the $Cr(CO)_3^-$ spectrum. Figure 8 compares photoelectron spectra obtained at 488 and 514 nm at a circulating laser power of about 40 W, recorded at an instrumental resolution of 9 meV. The spectra are plotted as a function of eKE between 0.2 and 2.4 eV and, thus, are shifted by the 0.131-eV difference in photon energy at these two wavelengths. At 488 nm, the 50× magnification reveals a weak, broad feature near 1.5 eV eKE. When the laser power is increased from 25 to 65 W, the intensity of this feature approximately doubles relative to that of the other peaks in the spectrum. This behavior suggests that this weak feature is due to a two-photon process involving photodissociation of $Cr(CO)_3^-$ followed by photodetachment of a fragment anion. At 514 nm, this feature appears with a greatly enhanced relative intensity, which does not, however, increase significantly when the laser power is doubled. In addition, spectra obtained for a mass-selected $Cr(CO)_2^-$ ion beam at 488 and 514 nm also show broad features in this region, whose intensities do not vary significantly with laser wavelength. These observations suggest that the broad features observed at high eKE in the spectra of the mass-selected $Cr(CO)_3^-$ ions are actually due to photodetachment from $Cr(CO)_2^-$ photofragments. In addition, the $Cr(CO)_3^- \rightarrow Cr(CO)_2^- + CO$ photodissociation cross section is evidently much greater at 514 nm than at 488 nm. An increase in the $Cr(CO)_3^-$ photodissociation cross section with increasing wavelength in this region was also observed in the photodisappearance ICR studies of Dunbar and Hutchinson.[23] Photofragmentation of $Cr(CO)_3^-$ to Cr^- also occurs at 514 nm, as is evident from the weak peak at 1.74 eV eKE, which is due to photodetachment from ground-state Cr^-.

Tables I–III list the main peaks observed in the 488-nm photoelectron spectra of $Cr(CO)_3^-$, $Mo(CO)_3^-$, and $W(CO)_3^-$. Positions, intensities, and widths (given as full widths at half maximum intensity relative to the local baseline) were obtained from least-squares fits of Lorentzian lineshapes to the observed peaks. Widths of shoulders due to excitation of the 480 cm^{-1} mode in $Cr(CO)_3^-$ and the CMC bending modes in $Mo(CO)_3^-$ and

Table I. Peak Positions in the $Cr(CO)_3^- \rightarrow Cr(CO)_3 + e^-$ Photoelectron Spectrum Obtained at 488 nm (2.540 eV)

electron kinetic energy (eV)	relative intensity (sh = shoulder)	width (FWHM, meV)	spacing from origin (cm^{-1})[a]	assignment
1.275	5	8	−680	2_1^0
1.191	1000	8	0	0_0^0
1.131	4 (sh)		480	3_0^1
1.107	120	9	680	2_0^1
1.023	5	9	1360	2_0^2
0.943	125	9	2000	1_0^1
0.883	1		2480	$1_0^1 3_0^1$
0.859	15	9	2680	$1_0^1 2_0^1$
0.776	1		3350	$1_0^1 2_0^2$
0.696	5	10	3990	1_0^2
0.612	1		4670	$1_0^2 2_0^1$

[a] Uncertainties in spacings are ±10 cm^{-1} for peaks whose widths are listed and ±20 cm^{-1} for other peaks.

Table II. Peak Positions in the $Mo(CO)_3^- \rightarrow Mo(CO)_3 + e^-$ Photoelectron Spectrum Obtained at 488 nm (2.540 eV)

electron kinetic energy (eV)	relative intensity (sh = shoulder)	width (FWHM, meV)	spacing from origin (cm^{-1})[a]	assignment
1.285	10	7	−660	2_1^0
1.216	70 (sh)		−100	4_1^0
1.203	1000	7	0	0_0^0
1.190	120 (sh)		100	4_0^1
1.178	20 (sh)		200	4_0^2
1.121	200	8	660	2_0^1
1.108	30 (sh)		770	$2_0^1 4_0^1$
1.040	20	8	1310	2_0^2
0.968	6 (sh)		1900	$1_0^1 4_1^0$
0.955	100	7	2000	1_0^1
0.943	10 (sh)		2100	$1_0^1 4_0^1$
0.874	20	8	2650	$1_0^1 2_0^1$
0.794	2	8	3300	$1_0^1 2_0^2$
0.708	4	12	3990	1_0^2

[a] Uncertainties in spacings are ±10 cm^{-1} for peaks with widths listed as 7–8 meV and ±20 cm^{-1} for other peaks.

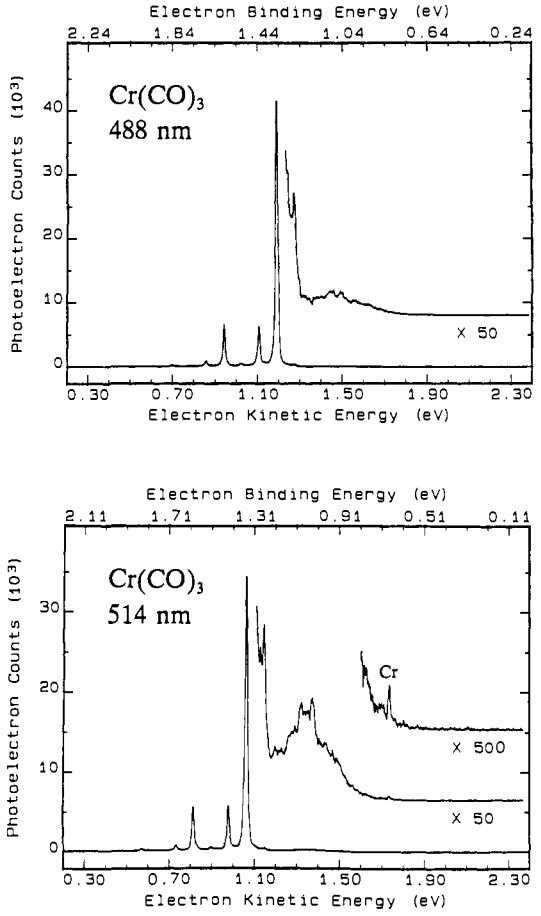

Figure 8. $Cr(CO)_3^- \rightarrow Cr(CO)_3 + e^-$ photoelectron spectra obtained at 488 (2.540 eV) and 514 nm (2.409 eV).

Table III. Peak Positions in the $W(CO)_3^- \rightarrow W(CO)_3 + e^-$ Photoelectron Spectrum Obtained at 488 nm (2.540 eV)

electron kinetic energy (eV)	relative intensity (sh = shoulder)	width (FWHM, meV)	spacing from origin (cm^{-1})[a]	assignment
0.759	15	7	−630	2_1^0
0.745	10	7	−520	see text
0.693	40 (sh)		−100	4_1^0
0.681	1000	8	0	0_0^0
0.668	100 (sh)		100	4_0^1
0.617	30 (sh)		520	$2_0^1 4_1^0$
0.604	300	8	620	2_0^1
0.590	40 (sh)		730	$2_0^1 4_0^1$
0.540	7 (sh)		1140	$2_0^2 4_1^0$
0.527	50	9	1240	2_0^2
0.513	7 (sh)		1360	$2_0^2 4_0^1$
0.446	10 (sh)		1900	$1_0^1 4_1^0$
0.433	130	8	2000	1_0^1
0.355	50	9	2630	$1_0^1 2_0^1$

[a] Uncertainties in spacings are ±10 cm^{-1} for clearly defined peaks and ±20 cm^{-1} for shoulders.

$W(CO)_3^-$ are not listed, as these were constrained in the fits to the widths of the stronger adjacent peaks. Widths are also not listed for several weak combination bands in the $Cr(CO)_3^-$ spectrum, due to uncertainties in baseline identification. Peak spacings from the origin band are given with an experimental uncertainty of ±10 cm^{-1} for narrow peaks and ±20 cm^{-1} for weak peaks and shoulders. Vibrational assignments are also given, using the notation $v_{v(\text{ion})}^{v(\text{neutral})}$, with the four observed vibrational modes numbered in order of decreasing frequency. For example, the peak at 0.696 eV eKE in the $Cr(CO)_3^-$ spectrum, labeled 1_0^2 in Table I, is assigned to a transition from the zero-point vibrational level of the anion to $v = 2$ of ν_1, the CO stretching vibration, in the neutral molecule.

Table IV. Summary of Electron Affinities and Vibrational Frequencies

	$Cr(CO)_3$	$Mo(CO)_3$	$W(CO)_3$
electron affinity (eV)	1.349 ± 0.006	1.337 ± 0.006	1.859 ± 0.006
fundamental freq (cm^{-1}) of A_1 modes[a]			
neutral molecule			
ν_1 (CO stretch)	2000 ± 10	2000 ± 10	2000 ± 10
ν_2 (MCO bend)	680 ± 10	660 ± 10	620 ± 10
ν_3 (MC stretch)	480 ± 20		
ν_4 (CMC bend)		100 ± 20	100 ± 20
negative ion			
ν_2 (MCO bend)	680 ± 10	660 ± 10	630 ± 10
ν_4 (CMC bend)		100 ± 20	100 ± 20

[a] The internal symmetry coordinate that makes the largest contribution to each normal mode, based on the potential energy distribution calculations described in section IV, is also indicated.

Table IV summarizes our measurements of the electron affinities of the neutral molecules and the fundamental frequencies of the symmetric vibrational modes of the neutral molecules and anions. On the basis of the results of the potential energy distribution calculations described in the next section, ν_2 is labeled as the symmetric MCO bend and ν_3 as the symmetric M–C stretch, although in each case the other internal coordinate makes a minor contribution to the normal mode.

IV. Force Constants and Geometry Changes

A. $Cr(CO)_3$. The principal CO stretching, CrC stretching, and CrCO bending force constants of neutral $Cr(CO)_3$ were estimated from the 2000 ± 10, 480 ± 20, and 680 ± 10 cm^{-1} vibrational frequencies measured here using the relation[52]

$$|\mathbf{GF} - \mathbf{\Lambda}| = 0$$

Since all of the observed modes correspond to A_1 vibrations and a C_{3v} $Cr(CO)_3$ molecule has four such vibrations, the **F** and **G** matrices in this equation are simply 4 × 4 symmetric matrices. **Λ** is a diagonal matrix whose elements are $\lambda_k = 4\pi^2\nu_k^2$, where ν_k is the fundamental frequency of vibrational mode k. Elements of the **G** matrix, which depend on the molecular structure and the atomic masses, were calculated by standard techniques[52] assuming a CCrC bond angle of 105°, as was determined for matrix-isolated $Mo(CO)_3$.[13] Bond lengths were assumed to be equal to those in $(C_6H_6)Cr(CO)_3$ (r_{CO} = 1.159 Å, r_{CrC} = 1.845 Å);[53,54] the use of $Cr(CO)_6$ bond lengths[55] (r_{CO} = 1.171 Å, r_{CrC} = 1.916 Å) did not significantly alter the results.

In the **F** matrix, each diagonal element involves both a principal valence force constant and an interaction constant. For example, $F_{1,1} = F_{CO} + 2F_{CO,C'O'}$, where $F_{CO,C'O'}$ represents the interaction of the stretching vibrations of two CO bonds. To obtain the principal force constants from the observed frequencies, we assumed the $F_{CO,C'O'}$, $F_{CrC,Cr'C'}$, and $F_{\beta\beta'}$ interaction constants (where $F_{\beta\beta'}$ represents the interaction of two MCO bends) to be equal to the values reported by Butler and co-workers[54] for (C_6H_6)-$Cr(CO)_3$; i.e., $F_{CO,C'O'}$ = 0.302 mdyn/Å, $F_{CrC,Cr'C'}$ = 0.285 mdyn/Å, and $F_{\beta\beta'}$ = 0.00 mdyn·Å/rad². To solve for the diagonal elements of the **F** matrix, we also constrained the off-diagonal interaction constants. As in the $(C_6H_6)Cr(CO)_3$ study, the CO stretching–CrC stretching interaction constants were assumed to be equal to their values[17] in $Cr(CO)_6$; i.e., $F_{CO,CrC}$ = 0.68 mdyn/Å for motions sharing a common carbon atom, and $F_{CO,Cr'C'}$ = −0.05 mdyn/Å for vibrations involving different carbons. In addition, the corresponding **F** matrix element ($F_{1,3} = F_{CO,CrC} + 2F_{CO,Cr'C'}$) was allowed to vary by ±0.1 mdyn/Å. The CrCO bending–CCrC bending interaction element was allowed to vary from −0.1 to +0.1

(52) Wilson, E. B., Jr.; Decius, J. C.; Cross, P. C. *Molecular Vibrations*; Dover: New York, 1955.
(53) (a) Bailey, M. F.; Dahl, L. F. *Inorg. Chem.* **1965**, *4*, 1314–1319. (b) Rees, B.; Coppens, P. *Acta Crystallogr.* **1973**, *B29*, 2515–2528.
(54) English, A. M.; Plowman, K. R.; Butler, I. S. *Inorg. Chem.* **1982**, *21*, 338–347.
(55) Whitaker, A.; Jeffery, J. W. *Acta Crystallogr.* **1967**, *23*, 977–984.

mdyn·Å/rad^2. Interaction constants between the CO stretch and the bending vibrations were assumed to be zero, as reported for the $M(CO)_6$ complexes.[17] Interaction constants between the MC stretch and the A_1 MCO and CMC bends in the C_{3v} complex, which could not directly be transferred from $Cr(CO)_6$ and were not reported for $(C_6H_6)Cr(CO)_3$, were also assumed to be zero.

With these assumptions, we obtain $Cr(CO)_3$ principal force constants of 15.1 ± 0.4 mdyn/Å for the CO stretch, 2.6 ± 0.3 mdyn/Å for the CrC stretch, and 1.10 ± 0.20 mdyn·Å/rad^2 for CrCO bending in the mirror plane. These uncertainties indicate the range of values obtained when all of the vibrational frequencies, including a presumed 100 ± 30 cm^{-1} value for the CCrC bending mode, are allowed to vary within their experimental uncertainties, and the CO stretching–CrC stretching and the CrCO bending–CCrC bending off-diagonal **F** matrix elements are each allowed to vary by ±0.1 unit as described above.

To characterize the A_1 normal modes of $Cr(CO)_3$ in terms of the molecule's internal symmetry coordinates, we used the resulting **F** matrix to calculate the potential energy distribution,[17]

$$V_{k1,\nu} = L_{k,\nu}F_{k1}L_{1,\nu}$$

where the **L** matrix and its transpose $\mathbf{L}^T$ are given by

$$\mathbf{L}^T\mathbf{F}\mathbf{L} = \mathbf{\Lambda}$$

Results indicate that the 2000 (ν_1), 680 (ν_2), and 480 (ν_3) cm^{-1} modes observed in the photoelectron spectrum are mainly (>80%) CO stretching, CrCO bending, and CrC stretching, respectively. In addition, ν_1 contains some contribution from CrC stretching, ν_2 is somewhat mixed with CrC stretching and CCrC bending, and ν_3 has some CO stretching and CrCO bending character.

The difference between the equilibrium geometry of the neutral $Cr(CO)_3$ molecule and that of the $Cr(CO)_3^-$ negative ion can be deduced from a Franck–Condon analysis of relative peak intensities observed in the photoelectron spectrum. Since the peak spacings reveal no detectable anharmonicity at our instrumental resolution, the vibrational modes were modeled as independent harmonic oscillators. Franck–Condon factors were computed using the recursion formula method of Hutchisson[56] as implemented by the least-squares spectral fitting program PESCAL.[57] The resulting normal mode displacements, in units of amu$^{1/2}$ Å, were 0.070 ± 0.015 for the CO stretching mode ν_1, 0.11 ± 0.02 for the CrCO bending mode ν_2, 0.025 ± 0.013 for the CrC stretching mode ν_3, and <0.2 for the CCrC bending mode ν_4.

To express these results in terms of changes in bond lengths and bond angles, the **L** matrix was used to convert the normal mode displacements, ΔQ, into internal symmetry coordinate displacements, ΔS:

$$\Delta S = \mathbf{L}\Delta Q$$

Results indicate that the absolute magnitude of the change in equilibrium geometry on detachment of an electron from the anion is 0.015 ± 0.004 Å for the CO bond length, 0.01 ± 0.01 Å for the CrC bond length, 1.7 ± 0.7° for the CrCO bond angle, and ≤1° for the CCrC bond angle. These uncertainties indicate the combined effects of the quoted experimental uncertainties in the normal mode displacements and force constants and of combining the contributions to each internal coordinate displacement from the different normal modes with arbitrary signs. Although the harmonic Franck–Condon analysis cannot itself disclose the directions of these geometry changes, some insight into this matter can be obtained from a consideration of the type of orbital associated with the extra electron, as is discussed in section V.

B. $Mo(CO)_3$. For $Mo(CO)_3$, principal CO stretching, MoCO bending, and CMoC bending force constants were estimated from the 2000 ± 10, 660 ± 10, and 100 ± 20 cm^{-1} fundamental vibrational frequencies observed in the photoelectron spectrum. The **G** matrix was calculated for a CMoC bond angle of 105°.[13] Bond lengths were initially set equal to those in $Mo(CO)_6$ (r_{CO} = 1.145 Å, r_{MoC} = 2.063 Å)[58] but were allowed to vary by ±0.05 Å. The $F_{CO,MoC}$, $F_{CO,Mo'C'}$, and $F_{\alpha\alpha'}$ constants (where $F_{\alpha\alpha'}$ represents the interaction between two CMoC bends) were constrained to 0.73 mdyn/Å, −0.05 mdyn/Å, and 0.13 mdyn·Å/rad^2, respectively, based on values[17] reported for $Mo(CO)_6$. Since the MoC stretching vibration of $Mo(CO)_3$ was not observed in the present study and since the principal MC stretching force constants of $Cr(CO)_6$ and $Mo(CO)_6$ are nearly the same (2.08 ± 0.08 and 1.96 ± 0.06 mdyn/Å, respectively),[17] the MoC stretching diagonal matrix element was assumed to be equal to that of $Cr(CO)_3$. The $F_{CO,C'O'}$ interaction constant was again constrained to the 0.302 mdyn/Å value reported for $(C_6H_6)Cr(CO)_3$; values[17] for $Cr(CO)_6$ (0.21 ± 0.03) and $Mo(CO)_6$ (0.22 ± 0.05) are equal to each other and slightly lower than that of the tricarbonyl complex. The $F_{\beta\beta'}$ interaction constant and the stretch–bend interaction constants were again assumed to be zero. As for $Cr(CO)_3$, the CO stretching–MoC stretching interaction matrix element was allowed to vary by ±0.1 mdyn/Å, and the MoCO bending–CMoC bending element was allowed to vary from −0.1 to 0.1 mdyn·Å/rad^2.

The resulting $Mo(CO)_3$ principal force constants are 15.2 ± 0.4 mdyn/Å for the CO stretch, 1.15 ± 0.25 mdyn·Å/rad^2 for the MoCO bend, and 0.5 ± 0.4 mdyn·Å/rad^2 for the CMoC bend. Again, these uncertainties indicate the combined effects of varying the vibrational frequencies, force constants, and geometries over the ranges indicated above. The large uncertainty in the CMoC bending force constant is mainly due to the ±20 cm^{-1} uncertainty in ν_4. Calculation of the **L** matrix indicates that the dominant internal coordinate contributions to the normal modes are the same as described for $Cr(CO)_3$. In addition, ν_4 is primarily the CMC bend but also contains some MCO bending contribution.

A Franck–Condon analysis of the $Mo(CO)_3^-$ photoelectron spectrum yielded normal mode displacements (amu$^{1/2}$ Å) of 0.065 ± 0.013 for ν_1, 0.14 ± 0.03 for ν_2, <0.03 for ν_3, and 0.21 ± 0.04 for ν_4. These values correspond to a 0.014 ± 0.004 Å change in r_{CO}, a 0.01 ± 0.01 Å change in r_{MoC}, a 2.1 ± 0.7° change in the MoCO bond angle, and a 1 ± 1° change in the CMoC bond angle on electron detachment.

C. $W(CO)_3$. Force constants for $W(CO)_3$ were estimated from the observed 2000 ± 10, 620 ± 10, and 100 ± 20 cm^{-1} vibrational frequencies. The same approximations were employed as in the $Mo(CO)_3$ analysis, but the $W(CO)_6$ interaction constants ($F_{CO,WC}$ = 0.79 mdyn/Å, $F_{CO,W'C'}$ = −0.08 mdyn/Å, and $F_{\alpha\alpha'}$ = ~0.14 mdyn·Å/rad^2)[17] and bond lengths (r_{CO} = 1.148 Å and r_{WC} = 2.058 Å)[58] were used. The W–C stretching mode was not observed in our studies; in $W(CO)_6$, the principal M–C stretching force constant (2.36 ± 0.04 mdyn/Å) is significantly larger than in $Cr(CO)_6$ (2.08 ± 0.08 mdyn/Å). Therefore, in the $W(CO)_3$ analysis, the corresponding **F** matrix element was allowed to vary from the value determined for $Cr(CO)_3$ to a value 20% higher. The resulting $W(CO)_3$ principal force constants were 15.2 ± 0.5 mdyn/Å for the CO stretch, 1.02 ± 0.25 mdyn·Å/rad^2 for the MCO bend, and 0.6 ± 0.5 mdyn·Å/rad^2 for the CMC bend. Differences in the bond lengths and bond angles of the negative ion and the neutral molecule were determined from the observed normal mode displacements of 0.080 ± 0.015, 0.20 ± 0.04, <0.03, and 0.23 ± 0.05 amu$^{1/2}$ Å for ν_1–ν_4, respectively. The results were 0.017 ± 0.004 Å for Δr_{CO}, 0.01 ± 0.01 Å for Δr_{WC}, 2.8 ± 1.0° for $\Delta\angle_{WCO}$, and 1 ± 1° for $\Delta\angle_{CWC}$.

Table V summarizes the force constants and geometry displacements obtained in these analyses.

V. Discussion

A. Anion Electronic Configuration. The very similar appearance of the $Cr(CO)_3^-$, $Mo(CO)_3^-$, and $W(CO)_3^-$ photoelectron spectra, which reflects similar structural displacements on electron detachment, suggests that the "extra" electron occupies the same type of molecular orbital in all three anions. One clue as to whether this orbital can be characterized as primarily a d or an s metal orbital is provided by a comparison of the electron affinity pattern within this series to that typically observed for triads of transition metal atoms.

(56) Hutchisson, E. *Phys. Rev.* **1930**, *36*, 410–420; **1931**, *37*, 45–50.
(57) Ervin, K. M.; Lineberger, W. C. Unpublished FORTRAN program.
(58) Arnesen, S. P.; Seip, H. M. *Acta Chem. Scand.* **1966**, *20*, 2711–2727.

Table V. Summary of Force Constants and Displacements[a]

	$Cr(CO)_3$	$Mo(CO)_3$	$W(CO)_3$
principal force constants for the neutral molecules			
$F_{CO\ stretch}$ (mdyn/Å)	15.1 ± 0.4	15.2 ± 0.4	15.2 ± 0.5
$F_{MC\ stretch}$ (mdyn/Å)	2.6 ± 0.3		
$F_{MCO\ bend}$ (mdyn·Å/rad²)	1.10 ± 0.20	1.15 ± 0.25	1.02 ± 0.25
$F_{CMC\ bend}$ (mdyn·Å/rad²)		0.5 ± 0.4	0.6 ± 0.5
normal mode displacements (amu$^{1/2}$ Å) between anion and neutral molecule[b]			
ΔQ (ν_1, CO stretch)	0.070 ± 0.015	0.065 ± 0.013	0.080 ± 0.015
ΔQ (ν_3, MC stretch)	0.025 ± 0.013	<0.03	<0.03
ΔQ (ν_2, MCO bend)	0.11 ± 0.02	0.14 ± 0.03	0.20 ± 0.04
ΔQ (ν_4, CMC bend)	<0.2	0.21 ± 0.04	0.23 ± 0.05
internal coordinate displacements between anion and neutral molecule			
Δr_{CO} (Å)	0.015 ± 0.004	0.014 ± 0.004	0.017 ± 0.004
Δr_{MC} (Å)	0.01 ± 0.01	0.01 ± 0.01	0.01 ± 0.01
$\Delta\angle_{MCO}$ (deg)	1.7 ± 0.7	2.1 ± 0.7	2.8 ± 1.0
$\Delta\angle_{CMC}$ (deg)	≤1	1 ± 1	1 ± 1

[a] See section IV for a description of the normal mode and Franck–Condon calculations used to obtain the principal force constants and internal coordinate displacements. [b] The internal symmetry coordinate that makes the largest contribution to each normal mode is also indicated.

For the purpose of this comparison, it is useful to distinguish between an atomic "s electron affinity"[50] for the process $M(s^1d^m) + e^- \rightarrow M^-(s^2d^m)$ and a "d electron affinity" for $M(s^2d^{m-1}) + e^- \rightarrow M^-(s^2d^m)$. The true electron affinity, which always refers to the ground states of the atom and the anion, may correspond to one of these values, depending on the ground-state electron configurations. For example, since the ground states of both W and W^- have s^2 configurations, the true electron affinity of W is the "d electron affinity", to which the atomic $s^2d^4 \rightarrow s^1d^5$ promotion energy[48] can be added to obtain the "s electron affinity". On the other hand, for Cr and Mo, which have s^1d^5 atomic and s^2d^5 anionic ground states, the true electron affinity is the s electron affinity, from which the d electron affinity can be obtained by adding the atomic $s^1d^5 \rightarrow s^2d^4$ promotion energy.

Accurate electron affinities have been measured spectroscopically for five complete transition metal triads.[47] Although a quick perusal of these values reveals no consistent pattern within each triad, a clear pattern emerges if we distinguish between s and d electron affinities. For the s electron affinities, all five triads exhibit a small (0.04–0.11 eV) increase from the first to the second transition series atom, followed by a large (0.44–1.01 eV) increase for the third transition series atom:

s Electron Affinities (eV)

I		II		III	
V	0.787	Nb	0.893	Ta	1.532
Cr	0.675	Mo	0.747	W	1.183
Co	1.094	Rh	1.137	Ir	1.916
Ni	1.181	Pd	1.238	Pt	2.128
Cu	1.235	Ag	1.302	Au	2.309

In contrast, for the d electron affinities, all five triads show a large (0.47–2.43 eV) increase from the first to the second transition series atom, followed by a large (0.71–1.61 eV) *decrease* from the second to the third transition series atom:

d Electron Affinities (eV)

I		II		III	
V	0.525	Nb	1.035	Ta	0.322
Cr	1.636	Mo	2.107	W	0.817
Co	0.662	Rh	2.714	Ir	1.565
Ni	1.156	Pd	3.536	Pt	2.230
Cu	2.624	Ag	5.052	Au	3.444

Within each triad, the third transition series atom has, by far, the largest s electron affinity, whereas the second transition series atom has, by far, the largest d electron affinity.

The same trends are observed if the electron affinities are given as a weighted average over the spin–orbit components[47,48] of the relevant states of the anion and the atom instead of using the lowest-energy spin–orbit component of each state, as was done above. In this case, a small increase of 0.03–0.12 eV is obtained in the s electron affinities on going from the first to the second transition series atom within each of the five triads, followed by a large increase of 0.44–1.01 eV for the third transition series atom. For the d electron affinities, one still obtains a large increase (0.54–2.55 eV) from the first to the second series atom, followed by a large decrease (0.61–1.41 eV) for the third series atom. Again, within each triad, the third transition series atom has, by far, the largest s electron affinity, whereas the second series atom has, by far, the largest d electron affinity.

These trends can be understood in part from a consideration of relativistic effects,[59] which are greatest for atoms of the third transition series. This phenomenon results in a contraction of the s (and, to a lesser extent, the p) orbitals, which have the greatest electron densities near the nucleus and thus the highest electron velocities. The smaller s and p orbitals more completely shield the d (and f) electrons from the nuclear charge, producing an expansion of those orbitals. Thus, relativistic effects result in more strongly bound s and p electrons, and more weakly bound d and f electrons, in metals of the third transition series.

To determine whether these atomic electron affinity patterns can be extended to molecular transition metal species, it is useful to consider the metal dimers Cu_2, Ag_2, and Au_2.[60] Like the $M(CO)_3^-$ systems studied here, the coinage metal dimers share a common ground-state valence electron configuration, and the extra electron occupies the same type of molecular orbital in all three anions. Since this is an sp hybrid orbital,[60] it may be expected that the electron affinities of these molecules will follow the characteristic s electron affinity pattern, with the third transition series dimer exhibiting a substantially higher electron affinity than the second. An examination of the measured electron affinities[60] of Cu_2 (0.836 ± 0.007 eV), Ag_2 (1.023 ± 0.007 eV), and Au_2 (1.938 ± 0.007 eV) confirms that this is indeed the case.

For the group VI tricarbonyls, we measure electron affinities of 1.349 eV for $Cr(CO)_3$, 1.337 eV for $Mo(CO)_3$, and 1.859 eV for $W(CO)_3$. Thus, the electron affinities are similar for the first and second transition series complexes and increase substantially for the third transition series complex. This pattern resembles that observed for the atomic s electron affinities, as well as for the coinage metal dimers, whose extra electrons occupy sp hybrid orbitals. On the basis of these considerations, it appears likely that the extra electron in the group VI $M(CO)_3^-$ anions occupies

(59) Pitzer, K. S. *Acc. Chem. Res.* **1979**, *12*, 271–276. Pyykkö, P.; Desclaux, J.-P. *Acc. Chem. Res.* **1979**, *12*, 276–281. Pyykkö, P. *Chem. Rev.* **1988**, *88*, 563–594.

(60) Leopold, D. G.; Ho, J.; Lineberger, W. C. *J. Chem. Phys.* **1987**, *86*, 1715–1726. Ho, J.; Ervin, K. M.; Lineberger, W. C. *J. Chem. Phys.* **1990**, *93*, 6987–7002.

a molecular orbital that is primarily a metal s or sp hybrid orbital, rather than a d orbital.

This assignment is supported by the similar relative photodetachment cross sections measured for the group VI tricarbonyls and for s electron detachments of the corresponding atomic metal anions. As has previously been pointed out,[50,61] negative ion photoelectron spectra often show significantly greater signal intensities for atomic transitions involving the detachment of s electrons than for d electron detachments. For example, the intensity of the peak due to the $^6S_{5/2} \rightarrow {}^5S_2$ s electron detachment in our atomic Cr^- spectrum is about 5 times greater than the combined intensities of the fine structure components of the $^6S_{5/2} \rightarrow {}^5D_J$ d electron detachment. For $Cr(CO)_3^-$, we find the integrated intensity of peaks in the spectrum to be equal, to within experimental error, to that of a Cr^- s electron detachment peak, when normalized to the same ion current and laser intensity.

If we assume, on the basis of the computational and indirect experimental evidence summarized in the Introduction, that the neutral group VI tricarbonyls have low-spin $^1A_1$ ground states, then the addition of an electron to an s or sp hybrid orbital yields $^2A_1$ ground states for the $M(CO)_3^-$ anions.

Previously reported semiempirical calculations indicate that the lowest unfilled orbitals in low-spin d^6 metal tricarbonyl fragments are a doubly-degenerate e set derived mainly from the metal d orbitals[31,32] and an a_1 hybrid orbital which involves a mixture of the valence p, s, and d_{z^2} metal orbitals (in order of decreasing contribution) with some delocalization to the carbonyl groups.[32] Of these two possibilities, our experimental results suggest that the latter provides the better description of the orbital occupied by the extra electron in the anion. Since single occupation of the doubly-degenerate d orbitals in a low-spin d^7 tricarbonyl is predicted[31] to yield a Jahn–Teller distorted geometry, the lack of spectral evidence for such a distortion in the $M(CO)_3^-$ anions provides further support for the conclusion that the extra electron occupies the a_1 hybrid orbital.

B. Geometry Displacements. The view that the extra electron in the $M(CO)_3^-$ anions occupies the sp hybrid orbital is also consistent with the observed structural changes on electron attachment. Since most of the electron density of this orbital is calculated[32] to point away from the $M(CO)_3$ fragment, the addition of an electron is expected to result in only small displacements between the equilibrium geometries of the anions and the corresponding neutral molecules, in agreement with the experimental results summarized in Table V.

The photoelectron data indicate a slight (0.01–0.02 Å) difference between the equilibrium CO bond lengths of the $M(CO)_3^-$ anions and the corresponding neutral molecules. Although the harmonic Franck–Condon analysis does not indicate the direction of this displacement, several considerations suggest that the CO bonds are longer in the anions. The extended Hückel calculations predict the a_1 hybrid orbital to be somewhat delocalized into the π^* orbitals of the carbonyl groups,[32] suggesting that the addition of an electron to this orbital will slightly weaken the CO bond. For $NiCO^-$,[36] as well, calculations[11b] indicate that the extra electron enters a vacant sp hybrid orbital pointed away from the metal carbonyl fragment, resulting in a slightly increased anion CO bond length. Singly-charged metal carbonyl anions studied by matrix IR spectroscopy exhibit CO stretching frequencies 110–160 cm^{-1} lower than those of the corresponding neutral molecules,[62] a result also suggestive of weaker, longer CO bonds in the anions.

The activity of the symmetric MCO bending mode in the photoelectron spectra indicates a small (1–4°) change in the equilibrium MCO bond angle in the mirror plane on electron detachment. This result implies that this angle deviates slightly from linearity in the neutral molecules and/or in the anions. It appears reasonable that the MCO bonds in these pyramidal tricarbonyl fragments may be slightly bent, in view of the similar results reported for many coordinatively saturated metal carbonyl complexes in which the symmetry about the MCO bond is lowered by the presence of a substituent. For example, X-ray and neutron diffraction studies of $(C_6H_6)Cr(CO)_3$ show significant (with respect to the quoted experimental uncertainties) deviations of 1.5–2.0° from linear MCO bonds.[53b] A gas-phase electron diffraction study of the C_{3v} $HCo(CO)_4$ molecule found equatorial MCO angles of 172.6 ± 1.2°, with the oxygen atoms bent toward the axial hydrogen.[63] An X-ray diffraction study of the isoelectronic $HFe(CO)_4^-$ ion also reported bent (~177°) MCO bonds.[64] Kettle has proposed a possible explanation based on σ–π^* electron repulsion for the occurrence of nonlinear MCO bonds in substituted metal carbonyl complexes with pyramidal $M(CO)_3$ groups.[30] Among the coordinatively unsaturated binary metal carbonyls, bent MCO bonds have been observed for VCO and $V(CO)_2$ in low-temperature matrix studies.[65,66] However, ab initio calculations[67] suggest that these systems have linear equilibrium geometries with very flat bending potentials.

C. Force Constants. The principal CO stretching force constants for the neutral tricarbonyls, obtained from the normal mode analyses described in section IV, are 15.1 ± 0.4 mdyn/Å for $Cr(CO)_3$, 15.2 ± 0.4 mdyn/Å for $Mo(CO)_3$, and 15.2 ± 0.5 mdyn/Å for $W(CO)_3$. These results can be compared with the corresponding values[17] of 17.24 ± 0.07 mdyn/Å for $Cr(CO)_6$, 17.33 ± 0.06 mdyn/Å for $Mo(CO)_6$, and 17.22 ± 0.04 mdyn/Å for $W(CO)_6$. The principal CO stretching force constants are essentially the same for the three metal complexes within each series, but are substantially lower in the tricarbonyl than the hexacarbonyl complexes. Consistent with this result, a monotonic reduction in CO stretching force constants with decreasing coordination number has been reported for a variety of unsaturated metal carbonyls studied by matrix infrared spectroscopy.[68,69] This reduction can be understood in terms of a greater metal electron density available for π back-bonding to the antibonding π^* orbitals of each ligand in the coordinatively unsaturated complexes, resulting in weaker C–O bonds.

Force constants for the low-frequency vibrational modes are also consistent with stronger metal–ligand bonding in the coordinatively unsaturated complexes. The MC stretching force constant measured here for neutral $Cr(CO)_3$, the only system for which this vibration is observed, is 2.6 ± 0.3 mdyn/Å, significantly higher than in $Cr(CO)_6$ (2.08 ± 0.08 mdyn/Å). The CO and MC stretching force constants of bare $Cr(CO)_3$ are similar to those of $(C_6H_6)Cr(CO)_3$ (15.41 and 2.40 mdyn/Å, respectively), in accord with the traditional model of this molecule as a $Cr(CO)_3$ group interacting with a benzene ring.[54]

For MCO bending in the mirror plane, we obtain principal force constants of 1.10 ± 0.20, 1.15 ± 0.25, and 1.02 ± 0.25 mdyn·Å/rad² for neutral $Cr(CO)_3$, $Mo(CO)_3$, and $W(CO)_3$, respectively. Similar values are expected for the anions, whose MCO bending frequencies are the same as those of the corresponding neutral molecules to within experimental error. These values exceed those of the corresponding hexacarbonyls (0.48 ± 0.07, 0.45 ± 0.03, and 0.48 ± 0.05 mdyn·Å/rad²), indicating a more rigid MCO bending potential in the tricarbonyls, again consistent with stronger metal–ligand π bonds in these systems. Large MCO bending force constants are also observed for $(C_6H_6)Cr(CO)_3$, for which values of 0.627 and 0.813 mdyn·Å/rad² are reported for bending parallel

(61) Engelking, P. C.; Lineberger, W. C. *Phys. Rev. A* **1979**, *19*, 149–155.
(62) Abel, E. W.; McLean, R. A. N.; Tyfield, S. P.; Braterman, P. S.; Walker, A. P.; Hendra, P. J. *J. Mol. Spectrosc.* **1969**, *30*, 29–50. Breeze, P. A.; Burdett, J. K.; Turner, J. J. *Inorg. Chem.* **1981**, *20*, 3369–3378.
(63) McNeill, E. A.; Scholer, F. R. *J. Am. Chem. Soc.* **1977**, *99*, 6243–6249.
(64) Smith, M. B.; Bau, R. *J. Am. Chem. Soc.* **1973**, *95*, 2388–2389.
(65) Hanlan, L.; Huber, H.; Ozin, G. A. *Inorg. Chem.* **1976**, *15*, 2592–2597.
(66) Van Zee, R. J.; Bach, S. B. H.; Weltner, W., Jr. *J. Phys. Chem.* **1986**, *90*, 583–588.
(67) Barnes, L. A.; Bauschlicher, C. W., Jr. *J. Chem. Phys.* **1989**, *91*, 314–330.
(68) DeKock, R. L. *Inorg. Chem.* **1971**, *10*, 1205–1211. Kündig, E. P.; McIntosh, D.; Moskovits, M.; Ozin, G. A. *J. Am. Chem. Soc.* **1973**, *95*, 7234–7241. Hanlan, L. A.; Huber, H.; Kündig, E. P.; McGarvey, B. R.; Ozin, G. A. *J. Am. Chem. Soc.* **1975**, *97*, 7054–7068. Ozin, G. A.; Hanlan, L. A. *Inorg. Chem.* **1979**, *18*, 2091–2101.
(69) Peden, C. H. F.; Parker, S. F.; Barrett, P. H.; Pearson, R. G. *J. Phys. Chem.* **1983**, *87*, 2329–2336.

to and perpendicular to the mirror plane, respectively.[54]

D. Bond Dissociation Energies. Rayner and co-workers[18] have recently reported estimates for the metal–ligand bond dissociation energies of the neutral group VI metal tricarbonyls based on time-resolved infrared spectroscopic studies of product branching ratios following UV photolysis of the stable hexacarbonyls. These results can be combined with the electron affinities (EA) measured in the present study to obtain the total metal–ligand bond energies in the anions, according to the following equation:

$$D_o[M(CO)_3^-] = D_o[M(CO)_3] - EA(M) + EA[M(CO)_3]$$

A comparison of the electron affinities of the metal atom and the corresponding tricarbonyl complex indicates that the sum of the three metal–ligand bond dissociation energies in the anion exceeds that of the corresponding neutral molecule by 0.674 ± 0.010 eV (15.5 ± 0.2 kcal/mol) for $Cr(CO)_3^-$, 0.590 ± 0.010 eV (13.6 ± 0.2 kcal/mol) for $Mo(CO)_3^-$, and 1.042 ± 0.010 eV (24.0 ± 0.2 kcal/mol) for $W(CO)_3^-$. The data reported by Rayner et al. (their Table I) yield average metal–ligand bond energies for the three M–CO bonds of 15.7 kcal/mol for $Cr(CO)_3$, 38.5 kcal/mol for $Mo(CO)_3$, and <45.7 kcal/mol for $W(CO)_3$.[18] Combining these results with the electron affinity values, we obtain average metal–ligand bond energies of 21 kcal/mol for $Cr(CO)_3^-$, 43 kcal/mol for $Mo(CO)_3^-$, and <54 kcal/mol for $W(CO)_3^-$. The former value is not consistent with the results of previously reported appearance potential measurements,[21] which indicated a much higher average bond energy of 30 kcal/mol for $Cr(CO)_3^-$.

The much greater difference between the total metal–ligand bond strengths of $W(CO)_3^-$ and $W(CO)_3$ (1.042 eV) than for the Cr and Mo tricarbonyls (0.674 and 0.590 eV, respectively) may at first seem surprising, in view of the similar geometry displacements between the neutrals and the anions of the three complexes. However, this apparent anomaly is easily explained on the basis of the different atomic ground states of W ($^5D_0$, s^2d^4) and of Cr and Mo ($^7S_3$, s^1d^5). If the bond dissociation energies of all three neutral $M(CO)_3$ complexes are referenced to the $^7S_3$ atomic states, then the difference between the $W(CO)_3^-$ and $W(CO)_3$ bond energies is reduced to 0.676 eV, a value similar to those of the other complexes. The greater metal–ligand bond dissociation energies of the anions than the neutral molecules are likely to be due in part to lower atomic promotion energies for the anionic than for the neutral systems, as well as to increased π-back-bonding in the anions.

VI. Summary

We have reported the 488-nm negative ion photoelectron spectra of $Cr(CO)_3^-$, $Mo(CO)_3^-$, and $W(CO)_3^-$ prepared at room temperature in a flowing afterglow ion source. The spectra of the group VI tricarbonyls, obtained at an instrumental resolution of 5 meV, are quite similar in appearance, suggesting that the extra electron occupies the same type of orbital in all three anions. Photodetachment transitions are observed to the ground electronic states of the neutral molecules and show weak vibrational activity in CO stretching and MCO bending modes and even weaker activity in MC stretching and CMC bending modes. The four active vibrational modes are assigned to the four A_1 modes of the C_{3v} molecules, implying that the anions also have C_{3v} equilibrium structures.

Force constants estimated for the neutral $M(CO)_3$ molecules from the fundamental vibrational frequencies measured here are consistent with stronger metal–ligand bonding in the coordinatively unsaturated complexes than in the corresponding hexacarbonyls. Franck–Condon analyses of the spectra indicate only small differences between the equilibrium bond lengths and bond angles of the anions and the corresponding neutral molecules. For example, displacements between the equilibrium structures of $Mo(CO)_3$ and $Mo(CO)_3^-$ are 0.014 ± 0.004 Å for the C–O bond length, ≤0.02 Å for the M–C bond length, 2.1 ± 0.7° for the MCO bond angle, and ≤2° for the CMC bond angle. Results for $Cr(CO)_3$ and $W(CO)_3$ do not differ from these significantly.

Electron affinities are measured to be 1.349 ± 0.006 eV for $Cr(CO)_3$, 1.337 ± 0.006 eV for $Mo(CO)_3$, and 1.859 ± 0.006 eV for $W(CO)_3$. A comparison of this electron affinity pattern to characteristic trends within triads of transition metal atoms, and within the coinage metal dimer series, suggests that the extra electron in the $M(CO)_3^-$ anions occupies a molecular orbital that is primarily a metal s or sp hybrid orbital, rather than an orbital of primarily metal d atomic parentage. This conclusion is also supported by photodetachment cross section measurements. Previously reported semiempirical calculations indicate that the lowest unfilled orbitals in low-spin d^6 metal tricarbonyl fragments are a doubly-degenerate e set derived mainly from the metal d orbitals[31,32] and an a_1 hybrid orbital which involves a mixture of the s, p, and d_{z^2} metal orbitals.[32] Of these possibilities, our experimental results suggest that the latter provides the better description of the orbital occupied by the extra electron in the anion. If the neutral tricarbonyls have $^1A_1$ ground states as is generally assumed, this assignment implies $^2A_1$ ground states for the $M(CO)_3^-$ anions.

The electron affinities measured here, combined with previously reported[18] bond energies for the neutral tricarbonyl complexes, yield average metal–ligand bond energies of 21 kcal/mol for $Cr(CO)_3^-$, 43 kcal/mol for $Mo(CO)_3^-$, and <54 kcal/mol for $W(CO)_3^-$.

Finally, we have described the design of a new continuous wave negative ion photoelectron spectrometer whose mass resolution is enhanced by an order of magnitude over that of previous instruments of this type. This improvement should make a wide range of organometallic fragments, including hydrogen-containing species, accessible to study by this powerful spectroscopic technique.

Acknowledgment. We are grateful for valuable advice on the design of our experimental apparatus from Professors Carl Lineberger, Kit Bowen, Barney Ellison, Kent Ervin, and Ron Gentry. The construction of this instrument would not have been possible without the expertise of shop personnel Harley Steinbrenner, Karl Lovgren, Bob Jones, Carl Johnson, and Bruce Moe. This research was supported by the NSF under PYI Grant CHE-8858373 and by generous matching grants from the Allied Signal, Amoco, Cray, Ford Motor, GE, IBM, and Newport Corporations. We also gratefully acknowledge support from the American Society for Mass Spectrometry, the Dreyfus Foundation, the Electric Power Research Institute, the McKnight Foundation, the donors of the Petroleum Research Fund, administered by the American Chemical Society, the Research Corporation under a Bristol-Myers Company grant, and the University of Minnesota.